DOI: 10.18721/JPM.13411
UDC 536.421

CURVED-RAY TENSOR TOMOGRAPHY FOR RESIDUAL STRESS MEASUREMENTS IN THE AXISYMMETRIC GRADED RODS

D.D. Karov[1], **A.E. Puro**[2]

[1] Peter the Great St. Petersburg Polytechnic University,
St. Petersburg, Russian Federation;

[2] Euroacademy, Tallinn, Estonia

For the first time, an algorithm for reconstructing an arbitrary distribution of residual stresses by the polarization tomography method for cylindrical rod structures with a radial distribution of the refractive index has been presented. The reconstruction took into account the ray refraction. The algorithm is based on the expansion of the tensor stress field in angular harmonics (singular value expansion). The case of an axisymmetric tensor field with an arbitrary stress gradient along the cylinder axis was considered. Numerical calculations were carried out for an axially symmetric stress distribution in a gradan for the case of a plane deformation state. The reconstruction was based on the expansion of the stress tensor in eigenfunctions of the boundary value problem. The regularized solution of the resolving equation (of Abelian type) used the expansion in the Zernike polynomials. The results of the reconstruction are given with taking into account the additional term due to the deflection of the transmission rays as well as without this doing.

Keywords: residual stress, integrated photoelasticity, transverse translucence, GRIN rod lense

Citation: Karov D.D., Puro A.E., Curved-ray tensor tomography for residual stress measurements in the axisymmetric graded rods, St. Petersburg Polytechnical State University Journal. Physics and Mathematics. 13 (4) (2020) 133–148. DOI: 10.18721/JPM.13411

This is an open access article under the CC BY-NC 4.0 license (https://creativecommons.org/licenses/by-nc/4.0/)

ТЕНЗОРНАЯ ТОМОГРАФИЯ ДЛЯ ИЗМЕРЕНИЯ ОСТАТОЧНЫХ НАПРЯЖЕНИЙ В ОСЕСИММЕТРИЧНЫХ ГРАДИЕНТНЫХ СТЕРЖНЯХ ПРИ ИСКРИВЛЕНИИ ПРОСВЕЧИВАЮЩИХ ЛУЧЕЙ

Д.Д. Каров[1], **А.Э. Пуро**[2]

[1] Санкт-Петербургский политехнический университет Петра Великого,
Санкт-Петербург, Российская Федерация;

[2] Евроакадемия, г. Таллинн, Эстония

Впервые представлен алгоритм реконструкции произвольного распределения остаточных напряжений методом поляризационной томографии для цилиндрических стержневых структур с радиальным распределением показателя преломления, с учетом рефракции лучей. Алгоритм основывается на разложении тензорного поля напряжений по угловым гармоникам (сингулярное разложение). Рассмотрен важный в прикладном плане случай осесимметричного тензорного поля при произвольном градиенте напряжений вдоль оси цилиндра. Численные расчеты проведены для аксиально симметричного распределения напряжений в градане для случая плоского деформированного состояния. Реконструкция основана на разложении тензора напряжений по собственным функциям краевой задачи. Регуляризованное решение разрешающего уравнения (Абелева типа) использует разложение по полиномам Цернике. Приводятся результаты реконструкции с учетом и без учета добавочного слагаемого, обусловленного отклонением просвечивающих лучей.

Ключевые слова: остаточное напряжение, интегральная фотоупругость, поперечное просвечивание, стержневая градиентная линза

Ссылка при цитировании: Каров Д.Д., Пуро А.Э. Тензорная томография для измерения остаточных напряжений в осесимметричных градиентных стержнях при искривлении просвечивающих лучей // Научно-технические ведомости СПбГПУ. Физико-математические науки. 2020. Т. 13. № 4. С. 133–148. DOI: 10.18721/JPM.13411

Статья открытого доступа, распространяемая по лицензии CC BY-NC 4.0 (https://creativecommons.org/licenses/by-nc/4.0/)

Introduction

Residual stress (RS) is one of the key characteristics describing the strength and optical quality of glass and crystal articles. Gradient refractive index (GRIN) structures, like rod lenses, laser rods, ball lenses, fiber preforms, and fibers have numerous applications. Most of them have an axially symmetric distribution of the refractive index that is the highest along its optical axis and decreases toward the periphery. A remarkably diverge range of optical profiling techniques has been developed during the last decades [1]; we assume in the discussion below that the refractive index (RI) n is known. Integrated photoelasticity [2] is a nondestructive method for stress analysis in 3D transparent specimens. This method consists in placing a 3D sample in an immersion bath ($n_{imm} = n_{surf}$; n_{imm}, n_{surf} are the RI of the immersion and product surface, respectively) and passing a beam of polarized light through the sample cross-section. Reconstruction of the spatial distribution of the stress tensor by interpreting the integrated optical effects of the rays that have passed through the medium may be considered a type of tensor field tomography [3]. It is based on solving the problem of optical tomography of the stress tensor field in combination with the resulting problem of elasticity theory. The problem of light propagation is separated into two parts [4] in the case of weak stresses (fiber preforms and fibers, GRIN lenses, laser rods): determining the ray paths in the GRIN structure and determining the change in the polarization of the light passed through a birefringent medium. As a rule, induced birefringence is rather weak in the GRIN structures, and it is possible to measure two linear integrals on each ray. One of them is connected with the transversal interaction of the 2D vector field and the other with the transversal interaction of the 2D tensor field. From a mathematical standpoint, we have the special case of tensor tomography with beam deflection [5, 6]. The reconstruction algorithm is based on circular harmonic decomposition (Cormac-type inversion) [7] of ray integrals. The inverse problem of reconstructing the RSs is actually divided into the following two successive stages [3] for rectilinear propagation of rays:

(*i*) reducing the tensor ray integrals to scalar ones,

(*ii*) determining all the stress-tensor components based on inverting the ray integrals and solving the corresponding thermoelasticity problem [8].

In contrast to polarimetric tomography of straight light rays, the tomographical problem and the inverse thermoelastic problem must be solved together in the GRIN media [9].

Below we will investigate two types of inverse problems.

The global inverse problem: tomographic measurements are performed in a system of parallel planes over the entire height of the sample (optical axis) (Fig. 1,*a*).

The local inverse problem: tomographic measurements are carried out in the two closely spaced sections orthogonal to the optical axis (Fig. 1,*b*).

The paper is structured as follows. The basics of tensor field tomography are introduced in the next section. In what follows, we give the algorithm of RS reconstruction. Appendix after the

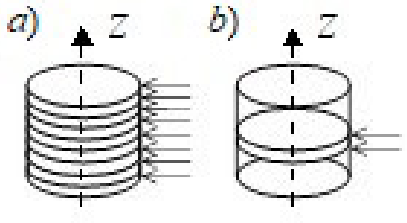

Fig. 1. Schematic drawing of the two raying methods corresponding to the global (*a*) and local (*b*) inverse problems

main material of the paper gives the singular decomposition of quasi-plane stresses in a circular cylinder.

Preliminaries

To make the presentation of our paper logical, we will give here the main concepts of tensor tomography of RS: the scalar and 2D-vector field tomography in the axially symmetric GRIN media and the main notions of the inverse thermoelasticity problem of integrated photoelasticity.

Ray equation in axially symmetric optical media. We will rely on the results obtained in the ray theory of axially symmetric optical media [10]. We use the Cartesian (x, y, z) coordinate system, as well as the cylindrical one (r, φ, z) and the moving one (s, α, z) associated with the measuring process (Fig. 2).

The axis z coincides with the axes of the cylinder. The cylinder is taken to have a unit radius. The ray is localized by its normal vector **s**, such that $\mathbf{s} = |\mathbf{s}|$ is the smallest distance from the ray to the origin, and θ is the angle between the **s** and the axis x (see Fig. 2). An arbitrary point on the ray is determined by its polar angle $\varphi = \theta \pm \alpha$ and by its distances r from the origin.

The RI $n(r)$ has rotational symmetry around the z-axis and $R(r) = n(r)r$ is a monotonic continuous function of r so that there is a one-to-one correspondence between R and r and only one ray passes through any two points inside the circle. We introduce another moving coordinate systems, (R, Ω, z) and (S, T, z), associated with the RI:

$$S(s) = sn(s),\ T = \pm\sqrt{R^2 - S^2},$$
$$\sin\Omega = \frac{T}{R},$$

where the plus sign holds for the left-hand side and minus for the right-hand side of the ray.

Then, the ray equation can be written in the next form:

$$\alpha\left[\left(R(r), S(s)\right]\right] = \pm\int_{|S|}^{r} \frac{S(s)\,d\rho}{\rho\sqrt{\left[R(\rho)\right]^2 - \left[S(s)\right]^2}} =$$
$$= \pm\int_{|S|}^{R} \frac{SD(K)\,dK}{K\sqrt{K^2 - S^2}} = A(R,S), \qquad (1)$$
$$D(R) = \frac{d\ln\left(r(R)\right)}{d\ln(R)},$$

where $\alpha(r,s) = \pm(\varphi(r) - \theta)$.

We give here also the formula for the differential of length l of an arc on the ray:

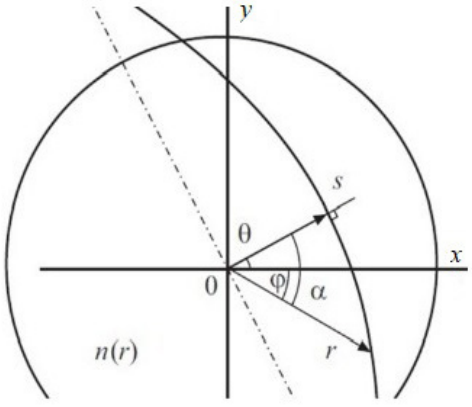

Fig. 2. The Cartesian (x, y, z), the cylindrical (r, φ, z) and the moving coordinate (s, α, z) systems used in the paper; the z-axis coincides with the axes of the cylinder; $\varphi = \theta \pm \alpha$ is the polar angle, $n(r)$ is a radial distribution of the refractive index

$$dl = \pm\sqrt{1+\left[r\frac{d\alpha}{dr}\right]^2}\,dr = \pm\frac{R(r)\,dr}{\sqrt{R^2(r)-S^2(s)}} = \\ = \pm\frac{L(R)\,RdR}{\sqrt{R^2-S^2}} = L(R)\,dT,\ L(R) = \frac{dr(R)}{dR}. \quad (2)$$

We assume that the RI is known and we can determine the ray equation.

Attenuated Radon transform in axially symmetric optical media. The Radon transform of $\hat{f}(s,\theta,\mu)$ with attenuation is defined here as follows [7]:

$$\hat{f}(s,\theta,\mu) = \int_{-l(s)}^{l(s)} f(s\boldsymbol{\theta}+\mathbf{x})\times \\ \times\exp\left(\int_0^l \mu(s\boldsymbol{\theta}+\mathbf{x})\,dk\right)dl,$$

where $l(s)$ is half the length of the ray in the circle, $\boldsymbol{\theta} = (\cos\theta, \sin\theta)$ is the unit vector along the s-axis, μ is the attenuation.

Let us transform the attenuation accumulated along the ray

$$M(R,S) = \int_0^l \mu(s\boldsymbol{\theta}+\mathbf{x})\,dk = \\ = \int_{|S|}^r \frac{\mu(k)R(k)\,dk}{\sqrt{\left[R(k)\right]^2-\left[S(s)\right]^2}} = \\ = \int_{|S|}^R \frac{\mu(K)L(K)Kdk}{\sqrt{K^2-S^2}} = M^0(T,S).$$

We can transform the ray integral by using polar coordinates (R, φ):

$$\hat{f}(S,\theta) = \int_S^{R_0} f\left[R,\theta+A(R,S)\right]\times \\ \times\frac{\exp\left[M(R,S)\right]L(R)\,RdR}{\sqrt{R^2-S^2}} + \\ + \int_S^{R_0} f\left[R,\theta-A(R,S)\right]\times \\ \times\frac{\exp\left[-M(R,S)\right]L(R)\,RdR}{\sqrt{R^2-S^2}}. \quad (3)$$

Applying the Radon transform for tomography of stress tensor fields in the optical glasses is connected with the circular harmonic decomposition (CHD) of stress functions [8, 9]. Expanding $f(r,\varphi)$ and $\hat{f}(S,\theta)$ in a Fourier series with respect to the corresponding angular variables, we obtain

$$f(r,\varphi) = \sum_{m=-\infty}^{\infty} f(r)e^{im\varphi}, \ldots \hat{f}(S,\theta) = \\ = \sum_{m=-\infty}^{\infty} g_m(S)e^{im\theta},$$

where

$$f_m(r) = \frac{1}{2\pi}\int_0^{2\pi} f(r,\varphi)e^{-im\varphi}d\varphi,$$

$$g_m(S) = \frac{1}{2\pi}\int_0^{2\pi} \hat{f}(S,\theta)e^{-im\theta}d\theta.$$

The absorption is imaginary in the problems of magneto-photoelasticity [11], in the studies of the magnetic field of the Tokamak plasma [12, 13], and in the magnetic resonance imaging [14]. Thus, we give the reconstruction algorithm for the case of imaginary attenuation, $\mu = i\eta$,

$$M(R,S) = \int_{|S|}^R \frac{i\eta(K)L(K)KdK}{\sqrt{K^2-S^2}} = iQ(R,S).$$

Inserting relationship (4) into a circular harmonic, we obtain

$$g_m(S,\eta) = \\ = 2\int_{|S|}^{R_0} \frac{\cos\left[E(m,K,S)\right]F_m(K)KdK}{\sqrt{K^2-S^2}}, \quad (4)$$
$$E(m,K,S) = mA(K,S)+Q(K,S),$$

an integral equation (generalized Cormack equation) for

$$F_m(R) = f_m(R)L(R).$$

The solution of Eq. (4) can be written as follows [7]:

$$f_m(r)n(r) = \frac{-1}{2\pi r}\left[\frac{\partial}{\partial r}\mathrm{Cr1}(qS,R,\eta) + \frac{m}{r}\mathrm{Sr1}(q,R,\eta)\right],$$

$$\mathrm{Cr1}(gS,R,\eta) = \mathrm{Cr}(gS,R,\eta) + \mathrm{Cr}(gS,R,-\eta),$$

$$\mathrm{Cr}(qS,R,\eta) = \int_R^{R_0} \frac{\mathrm{ch}\left[G(m,S,R,\eta)\right]}{\sqrt{S^2-R^2}} q_m(S,\eta)SdS,$$

$$G(m,S,R,\eta) = mB(S,R) + N(s,R), \quad (5)$$

$$B(S,R) = \int_R^{|S|} \frac{SD(K)dK}{K\sqrt{S^2-K^2}},$$

$$N(S,R) = \int_R^{|S|} \frac{\eta(K)L(K)KdK}{K\sqrt{S^2-K^2}},$$

$$\mathrm{Sr1}(g,R,\eta) = \mathrm{Sr}(g,R,\eta) + \mathrm{Sr}(g,R,-\eta),$$

$$\mathrm{Sr}(q,R,\eta) = \int_R^{R_0} \mathrm{sh}\left[G(m,S,R,\eta)\right] q_m(S,\eta)dS.$$

We write it in a more familiar form:

$$f_m(r) = \frac{-1}{2\pi}\frac{dR(r)}{dr} \times \left\{\left[\mathrm{Cr1}(g'_m,R,\eta)\right] + \left[\mathrm{Sr2}(r,\eta) + \mathrm{Sr2}(r,-\eta)\right]\right\},$$

$$\mathrm{Sr2}(R,\eta) = \int_R^{R_0} \frac{\mathrm{sh}\left[G(m,S,R,\eta)\right]}{\sqrt{S^2-R^2}} q_m(S,\mu) \times \left[m\int_R^S \frac{D'(K)dK}{\sqrt{S^2-K^2}} + \int_R^S \frac{S\left[\eta(K)L(K)\right]' dK}{\sqrt{S^2-K^2}}\right] dS.$$

The operator Sr2 consists of the part connected with the ray curvature (it is proportional to the harmonic number m) and the part connected with attenuation (the second integral in square brackets). It means that this part can be neglected if the angle variation of the field is small (m is small).

Cormack-type inversion of attenuated ray integral of a vector function. Reconstruction of stresses is connected with the reconstruction of vector fields. According to the Helmholtz theorem, any vector field $\mathbf{W}(r, \varphi)$ can be split up into a curl-free component and a source-free one:

$$\mathbf{W} = W_n\mathbf{e}_n + W_l\mathbf{e}_l = \left(\frac{\partial\tau}{\partial n} + \frac{\partial N}{\partial l}\right)\mathbf{e}_n + \left(\frac{\partial\tau}{\partial l} - \frac{\partial N}{\partial n}\right)\mathbf{e}_l.$$

where τ, N are the potentials of these components; $\mathbf{e}_n$, $\mathbf{e}_l$ denote the unit normal and unit tangent vectors to our curves.

For simplicity, we suppose that

$$\tau(1,\varphi) = N(1,\varphi) = 0$$

have homogeneous boundary conditions, obtained in the case of reconstructions of quasi-plane deformation.

The measurements in the linear vector tomography can be represented by a ray path integral in the form of a scalar (inner) product of a "probe" vector $\mathbf{p}$ and vector $\mathbf{W}$ as

$$\int_{-l(s)}^{l(s)} \mathbf{pW}(s\boldsymbol{\theta} + \mathbf{x}) \times$$

$$\times \exp\left(i\int_0^l \eta\left(s\boldsymbol{\theta}+\mathbf{x}\right)dk \right)dl.$$

The special case when $\mathbf{p} = \mathbf{e}_l$ is what H. Braun and A. Hauck [15] call the longitudinal measurements, and this leads to the formula

$$\hat{W}_l = -\int_{-l(s)}^{l(s)} \left[\frac{\partial N}{\partial n} + i\eta\tau \right] \times \\ \times \exp\left(i\int_0^l \eta\left(s\boldsymbol{\theta}+\mathbf{x}\right)dk \right)dl \qquad (6)$$

with applications to the Doppler tomography of a velocity field. Here we transform the ray path integral by partial integration.

Another special case when $\mathbf{p} = \mathbf{e}_n$ gives the transverse measurements:

$$\hat{W}_n = \int_{-l(\theta)}^{l(\theta)} \left[\frac{\partial \tau}{\partial n} - i\eta N \right] \times \\ \times \exp\left(i\int_0^l \nu\left(s\boldsymbol{\theta}+\mathbf{x}\right)dk \right)dl, \qquad (7)$$

which is essential for reconstructing the shear stresses.

A simple analogy between Eqs. (6), (7) is evident. Thus, only the application of Cormack-type inversion to the transverse vector integral (7) can be described. It can be written as the sum of two integrals:

$$\hat{W}_n = \\ = \int_{-l(s)}^{l(s)} \left[\frac{\partial \tau}{\partial n} \right] \exp\left(i\int_0^l \eta\left(s\boldsymbol{\theta}+\mathbf{x}\right)dk \right)dl - \qquad (8) \\ - i\int_{-l(s)}^{l(s)} \eta N \exp\left(i\int_0^l \eta\left(s\boldsymbol{\theta}+\mathbf{x}\right)dk \right)dl.$$

The first one is transformed using cylindrical coordinates:

$$\frac{\partial \tau}{\partial n} = \sin\nu \frac{\partial \tau}{\partial r} + \cos\nu \frac{\partial \tau}{r\partial \varphi},$$

$$\sin\nu = \frac{S(s)}{R(r)} = \cos\Omega,$$

$$\cos\nu = \pm \frac{1}{R(r)} \sqrt{R^2(r) - S^2(s)},$$

where the plus sign holds for the left-hand side and minus for the right-hand side of the ray.

Expanding $\tau(R, \varphi)$, $\eta(R, \varphi)$, $N(R, \varphi)$ and $\hat{W}_n(s,\theta)$ in Fourier series, namely

$$\tau(R,\varphi) = \sum_{m=-\infty}^{\infty} \tau_m(R) e^{im\varphi},$$

$$\eta(R,\varphi) N(R,\varphi) = \sum_{m=-\infty}^{\infty} N_m(R) e^{im\varphi},$$

$$\hat{W}_n(S,\theta) = \sum_{m=-\infty}^{\infty} w_m(S) e^{im\theta},$$

we can transform integral equation (8) to the following form:

$$w_m(S) = w_m^1(S,\tau) + w_m^2(S,N),$$

$$w_m^1(S,\tau) = 2\int_{|S|}^{R_0} \frac{\cos\left[E(m,K,S)\right] S}{\sqrt{K^2 - S^2}} \frac{d\tau_m(K)}{dK} + \\ + \frac{m\sin\left[E(m,K,S)\right]}{k(K)} \frac{dk(K)}{dK} \tau_m(K) dK, \qquad (9)$$

$$w_m^2(S,N) = \qquad (10)$$

$$= 2\int_{|S|}^{R_0} \frac{\cos\left[E(m,K,S)\right] N_m(K) L(K) K}{\sqrt{K^2 - S^2}} dK.$$

The reconstruction of potential τ is carried out by the operator [7]:

$$\tau_m(R) = -\frac{1}{\pi} \mathrm{Cr1}\left(w_m^1, R, \eta\right). \qquad (11)$$

As integral (10) coincides with Eq. (4), we can reconstruct $N_m(R)$ by using Eq. (5) for reconstruction of the scalar function [7].

Invariant representation of the stress tensor field in the inverse thermoelasticity problem. Most of the GRIN structures are formed by the ion-exchange method based on diffusion in alkali-containing glasses. There are two possi-

ble sources of RSs produced by varying the glass composition: the size difference between the exchange and the diffusing ions, and the radial variation in the coefficient of thermal expansion across the gradient region. As the lens cools from the ion-exchange temperature to room temperature, RS is introduced. In general, the tensor of residual deformation is the reason for RSs; the components of this tensor do not satisfy the compatibility equations. In the case of ordinary glass, the tensor of residual deformation can be considered to be spherical. Such an isotropic dilation field can be described by a certain "fictive" temperature field [16], and determination of RS can be connected with the solution of the thermoelasticity problem. The problem of reconstructing the thermal residual stresses using integrated photoelasticity is called the inverse thermoelasticity problem of optical tomography [8]. It is assumed in this model that the stress tensor $\boldsymbol{\sigma}$ obeys the equilibrium equations div $\sigma = 0$. The lateral surface of a cylinder is free from loads.

Let us use stress functions Φ, τ, N for the representation of RSs:

$$\sigma_{rr} = \left[\frac{1}{r}\frac{\partial}{\partial r} + \frac{1}{r^2}\frac{\partial^2}{\partial \varphi^2}\right]\Phi - \\ -\frac{\partial}{\partial z}\tau + 2\frac{\partial}{\partial r}\left[\frac{1}{r}\frac{\partial}{\partial \varphi}N\right],$$

$$\sigma_{r\varphi} = -\frac{\partial}{\partial r}\left[\frac{1}{r}\frac{\partial}{\partial \varphi}\Phi\right] - \\ -r\frac{\partial}{\partial r}\left[\frac{1}{r}\frac{\partial}{\partial r}\right]\Phi - \frac{1}{r^2}\frac{\partial^2}{\partial \varphi^2}N, \qquad (12)$$

$$\sigma_{\varphi\varphi} = \left[\frac{\partial^2}{\partial r^2}\right]\Phi - \frac{\partial}{\partial z}\tau - \\ -2\frac{\partial}{\partial r}\left[\frac{1}{r}\frac{\partial}{\partial \varphi}N\right],$$

$$\sigma_{rz} = \frac{\partial}{\partial r}\tau + \frac{\partial}{r\partial \varphi}N,$$

$$\sigma_{\varphi z} = \frac{\partial}{r\partial \varphi}\tau - \frac{\partial}{\partial r}N.$$

It was established [8] that the following stressed states are possible in a sample: (*i*) a quasi-planar stressed state caused by residual deformations ($N = 0$); (*ii*) a torsional stressed state caused by external loads ($\Phi = \tau = 0$), and (*iii*) a superposition of the aforementioned stresses (a quasi-torsional deformation). The state of pure torsion cannot be generated by a thermal source alone. Therefore, the first and third types of stresses are to be reconstructed.

We have also two additional equations for the reconstruction of the quasi-plane stress state:

$$\Delta_+\Phi = \left[\frac{\partial^2}{\partial r^2} + \frac{1}{r}\frac{\partial}{\partial r} + \frac{1}{r^2}\frac{\partial^2}{\partial \varphi^2}\right]\Phi = \\ = \sigma_{zz} + \Psi(x, y, z), \\ \Delta_+\tau = -\frac{\partial}{\partial z}\sigma_{zz}, \qquad (13) \\ \left(\Delta_+ + \frac{\partial^2}{\partial z^2}\right)\Psi = \Delta\Psi = 0,$$

and the equation for determining quasi-torsional stresses $\Delta N = 0$.

Here Ψ is a 3D harmonic function, connected with boundary conditions. It was proved that the quasi-planar stress ($N = 0$, $\Psi = 0$) can be determined locally based on the values of axial stress and its two first derivatives along the direction of the axis. Moreover, it can be seen from Eqs. (13) that in this case,

$$\frac{\partial}{\partial z}\Phi(x, y, z) = -\tau(x, y, z).$$

In particular, it was confirmed that the thermal stresses of the first angular harmonic are completely reconstructed by the local method. The quasi-torsional stresses can be reconstructed by the global method. The magnitude of the quasi-torsional stresses is almost negligibly small in comparison with quasi-plane stresses and we will

confine our attention mainly to reconstructing quasi-plane stresses ($N = 0$, $\Psi = 0$).

Algorithm for reconstruction of residual stresses

Since the reconstruction of RS is based on solving the problem of optical tensor tomography of the stress tensor field together with the problem of elasticity theory, let us first consider the tomographical problem.

Ray integrals of polarized tomography. Transformation of light polarization is measured in a plane orthogonal to the axis of the cylinder. Because there is added torsion of the ray in the plane of transillumination, variations in the polarization within the quasi-isotropic approximation are governed by the following system of equations [9]:

$$\frac{d}{dl}\mathbf{E} = -iCP\mathbf{E}, \qquad \mathbf{E} = \begin{bmatrix} E_z \\ E_s \end{bmatrix}, \tag{14}$$

$$P = \begin{bmatrix} 0.5\left(\sigma_{zz} - \sigma_{nn}\right) & \sigma_{nz} \\ \sigma_{nz} & 0.5\left(\sigma_{nn} - \sigma_{zz}\right) \end{bmatrix},$$

where $\mathbf{E}$ is the vector representing the amplitude of the electric field strength (the Jones vector), σ_{kj} are the stress tensor components in the moving system coordinates $\mathbf{e}_n$, $\mathbf{e}_l$, $\mathbf{e}_z$ (the Frenet – Serret frame), C is the photoelastic constant.

The solution of Eqs. (14) in the linear approximation can be represented as two ray integrals along the ray [2, 3]:

$$2\gamma\cos\psi = C\int_{-l(s)}^{l(s)}\left(\sigma_{zz} - \sigma_{nn}\right)dl = \\ = CH_0\left(s,\theta\right), \tag{15}$$

$$\gamma\sin\psi = C\int_{-l(s)}^{l(s)}\sigma_{nz}\,dl = \\ = CH_1\left(s,\theta\right), \tag{16}$$

where γ is the integrated optical retardation, ψ is the isocline parameter [2].

These parameters can be measured experimentally and form the physical foundation of the tomography. The ray integral (15) is connected with transversal interaction of the 2D tensor field in the plane of transillumination and the other one (16) is connected with transversal interaction of the 2D vector field (σ_{xz}, σ_{yz}). The cylindrical coordinate system is the most convenient for solving the inverse thermoelastic problem of the cylinder. Thus, we rewrite stress tensor components in cylindrical coordinates:

$$\sigma_{nn} = \sigma_{rr}\cos^2\beta + \sigma_{\varphi\varphi}\sin^2\beta + 2\sigma_{r\varphi}\sin\beta\cos\beta,$$

$$\sigma_{nz} = \sigma_{zr}\cos\beta + \sigma_{\varphi z}\sin\beta.$$

where β is the angle between the normal to a ray and the θ-axis.

Further, using the relations

$$\beta = \nu - \frac{\pi}{2},$$
$$\sin\beta = -\cos\nu, \quad \cos\beta = \sin\nu$$

we transform them to the following form:

$$\sigma_{nn} = \sigma_{rr}\sin^2\nu + \sigma_{\varphi\varphi}\cos^2\nu - \\ - 2\sigma_{r\varphi}\sin\nu\cos\nu, \tag{17}$$
$$\sigma_{nz} = \sigma_{zr}\sin\nu - \sigma_{\varphi z}\cos\nu.$$

Let us rewrite stresses (17) in terms of stress functions (12):

$$\sigma_{nn} = -\frac{\partial}{\partial z}\tau + \sigma_{nn}\left(\Phi\right) + \sigma_{nn}\left(N\right),$$

$$\sigma_{nn}\left(\Phi\right) = \sin^2\nu\left[\frac{1}{r}\frac{\partial}{\partial r} + \frac{1}{r^2}\frac{\partial^2}{\partial\varphi^2}\right]\Phi + \\ + \cos^2\nu\left[\frac{\partial^2}{\partial r^2}\right]\Phi + \sin 2\nu\frac{\partial}{\partial r}\left[\frac{1}{r}\frac{\partial}{\partial\varphi}\Phi\right],$$

$$\sigma_{nn}(N) = 2\sin^2\nu\frac{\partial}{\partial r}\left[\frac{1}{r}\frac{\partial}{\partial\varphi}\right] - 2\cos^2\nu\frac{\partial}{\partial r}\left[\frac{1}{r}\frac{\partial}{\partial\varphi}N\right] + \sin 2\nu\left[r\frac{\partial}{\partial r}\left[\frac{1}{r}\frac{\partial}{\partial r}\right] - \frac{1}{r^2}\frac{\partial^2}{\partial\varphi^2}\right]N, \quad (18)$$

$$\sigma_{nz} = \sin\nu\left[\frac{\partial}{\partial r}\tau + \frac{1}{r}\frac{\partial}{\partial\varphi}N\right] - \cos\nu\left[\frac{1}{r}\frac{\partial}{\partial\varphi}\tau - \frac{\partial}{\partial r}N\right].$$

The magnitude of quasi-torsion stresses is almost negligibly small in comparison with quasi-plane stresses, and below we consider the case of quasi-plane deformation: $N = 0, \Phi(1) = \partial\Phi/\partial r = 0$.

The first ray integral in the space of angular harmonics can be written as

$$\hat{H}_0(m,S) = \hat{\sigma}_{zz}(m,S) - \frac{\hat{\partial}\tau}{\partial z} - \hat{\sigma}_{nn}(m,S), \quad (19)$$

$$\hat{\sigma}_{nn}(S,m) = -2\int_S^{R(1)} \frac{\cos\left[mA(R,S)\right]}{\sqrt{R^2 - S^2}} \times \left\{\sin^2\nu\left[\frac{1}{r}\frac{\partial}{\partial r} - \frac{m^2}{r^2}\right]\Phi_m + \cos^2\nu\left[\frac{\partial^2}{\partial r^2}\right]\Phi_m\right\} Rdr - 2m\int_S^{R(1)} \frac{\sin\left[mA(R,S)\right]}{\sqrt{R^2 - S^2}} \times \sin 2\nu\frac{\partial}{\partial r}\left[\frac{1}{r}\Phi_m\right] Rdr. \quad (20)$$

Integrating by parts, we transform Eq. (20) to the formula

$$\hat{\sigma}_{nn}(S,m) = -2\int_S^{R(1)} \frac{\cos\left[mA(R,S)\right]}{\sqrt{R^2 - S^2}} \times \frac{S^2}{R^2}\left(\frac{\partial}{\partial r}\Phi_m\right)\left(\frac{d}{dr}n(r)\right) rdr - 2m\int_S^{R(1)} \sin\left[mA(R,S)\right] \times \frac{S}{R^2}\Phi_m\left(\frac{d}{dr}n(r)\right) dr, \quad (21)$$

containing in an explicit form the term $dn(r)/dr$ depending on the curvature of the ray.

The second ray integral (16) is connected with transversal interaction of the two-dimensional vector field and coincides with Eq. (11) in a space of angular harmonics:

$$\hat{H}_1(S,m) = \hat{\sigma}_{nz}(S,m) = w_m^1(S,\tau), \quad (22)$$

Thus, for stress reconstruction, we have four equations: two differential (Eqs. (13)) and two integral (Eqs. (19), (22)) ones.

The problem of reconstructing the RSs in the global and the local forms. Tomographic measurements in the global inverse problem are performed in a system of parallel planes over the entire height of the cylinder. The layer-by-layer reconstruction of stresses is possible starting from the bottom of the cylinder, where the axial stress is zero. Thus, we can determine τ from Eq. (22), the normal stress σ_{zz} and Φ using Eq. (13) and then all stress components given by Eqs. (12). The first ray integral (15) is not used in this algorithm.

Although the presented algorithm includes, as a special case, rectilinear propagation of rays, numerical implementation of the algorithm may differ for these cases. More detailed analysis shows that the global approach allows for reconstructing stresses completely [8].

Tomographic measurements in the local inverse problem are carried out in two closely spaced sections orthogonal to the optical axis for determining the height derivative of τ. Quasi-plane stresses are determined based on two differential Eqs. (13) and two ray integrals (19), (22).

Reconstruction of the quasi-plane stresses in the GRIN structures. For regularization of the inverse problem, we use singular decomposition of

the solution of Eqs. (13). The angular decomposition using trigonometric functions and radial decomposition using the Zernike polynomials were applied to represent the stresses (see Appendix) [8, 17]. MATLAB codes were developed to numerically solve integral Eqs. (19), (22) by the least square method. This method has been previously used for inversion of the Abel transform [18, 19]. We have three types of unknown coefficients:

$$\sigma_{zzm}^{kc,s}, \frac{\partial}{\partial z}\sigma_{zzm}^{kc,s}, \frac{\partial^2}{\partial z^2}\sigma_{zzm}^{kc,s}.$$

The second type of them can be determined from Eq. (22). The integrals

$$w_m^k(S) = 2\int_{|S|}^{1} \frac{\cos\left[mA(R,S)\right]S}{\sqrt{R^2-S^2}} \frac{d\tau_m^{k1}(r)}{dr} + \frac{m\sin\left[mA(R,S)\right]}{r}\tau_m^{k1}(r)\,dr,$$

$$\tau_m^{k1}(r) = \frac{1}{2m}\left[C_k^m(r) + D_k^m(r)\right],$$

$$\frac{\partial}{\partial r}\tau_m^{kc,s}(r) = \frac{-1}{2\rho}\left[C_k^m(r) - D_k^m(r)\right]$$

have to be calculated for the inversion Eq. (9).

According to the least-squares method [19], in order to determine $\frac{\partial}{\partial z}\sigma_{zzm}^{kc,s}$ we solved the following equation:

$$\sum_{n=1}^{N}\left[\hat{H}_1(S_n,m) - w_m^k(S_n)\frac{\partial}{\partial z}\sigma_{zzm}^{kc,s}\right]^2 = \min,$$

where S_n are the n measured points, $\hat{H}_1(S_n, m)$ is the measured ray integral.

The number of polynomials in the representation is connected with noise filtering. The second derivative $\partial^2\sigma_{zzm}^{kc,s}/\partial z^2$ can be approximately determined by measuring integrals in two parallel closely spaced sections. Then we can determine $\sigma_{zzm}^{kc,s}$ using solution (21).

Two types of refractive index profiles have been used in MATLAB codes [20, 21]. The profile of GRIN structures

$$n(r/R) = n_0\sqrt{1-g(r/R)^2}$$

is known as the parabolic refractive index profile [21]. Here n_0 is the refractive index on the axis and g is a positive constant, R is the radius of the cylinder.

In this case, the ray equation (1) has an analytical solution:

$$\alpha(r,s) = \arccos\left[\frac{s}{r}\sqrt{\frac{R^2-g(r^2+s^2)}{R^2-2gs^2}}\right].$$

The Cartesian coordinates of these rays can be expressed analytically in terms of the parameters r, s:

$$y(r,s) = s\sqrt{\frac{R^2-g(r^2+s^2)}{R^2-2gs^2}},$$

$$x(r,s) = \sqrt{\frac{(r^2-s^2)(R^2-gs^2)}{R^2-2gs^2}}.$$

It is clear that $g < 0.5$ here. These relations are used for ray tracing and solutions (19), (22) if $m > 0$.

Another profile (parabolic) of the form

$$n(r) = n_0\left[1-0.5g^2(r/R)^2\right]$$

is typically used to approximate the index refraction of GRIN lenses [21, 22] and of multimode fibers. The parameter g varies from 0.01 for fibers up to 0.30 for GRIN rod lenses.

Ray tracing is given for the case $g = 0.2$ (Fig. 3). The angle (1) can be expanded using the small parameter g. The expansion to within the first two terms

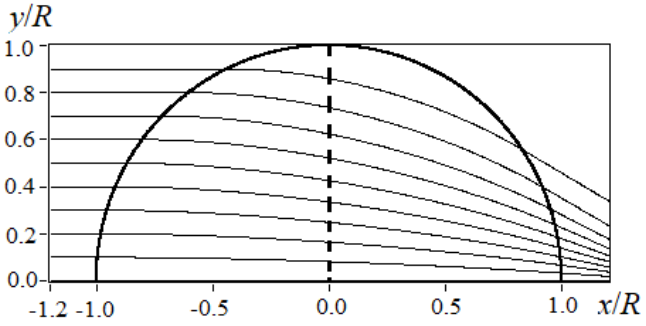

Fig. 3. Ray tracing through the sample (its half-round cross-section of diameter $2R$ is shown) when $n\,(r/R) = n_0[(1 - 0.2(r/R)^2]^{1/2}$ ($g = 0.2$, x is the translucence parameter)

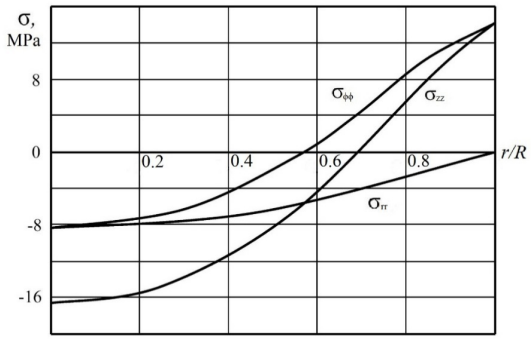

Fig. 4. The reconstructed principal components of the stress tensor over the GRIN lense's radius (the lense was made of zirconium-silicate glass)

$$\alpha(r,s) = \pm\int_{|S|}^{r} \frac{S(s)\,d\rho}{\rho\sqrt{\left[R(\rho)\right]^2 - \left[S(s)\right]^2}} \approx$$

$$\approx \pm\int_{|S|}^{r} \frac{s\,d\rho}{\rho\sqrt{[\rho]^2 - [s]^2}} =$$

$$= \pm 0.5\left(\frac{g}{R}\right)^2 s\sqrt{r^2 - s^2}$$

coincides with the expansion of

$$\alpha_1 = \arccos\left[\frac{S_1(s)}{R_1(r)}\right],$$

$$R_1(r) = n_0\left[R^2 + 0.5g^2r^2\right]r,$$

$$S_1(s) = n_0\left[R^2 + 0.5g^2s^2\right]s.$$

This approximation can be used in practice to solve Eqs. (19), (22) if $g < 0.1$ and $m < 15$. The algorithm of reconstruction is simplified [9] for axial symmetric plane-strain state ($m = 0$). In this case, all functions depend only on the radial coordinates, and we take only Eq. (19):

$$\hat{H}_0(s) =$$

$$= 2\int_{|S|}^{1}\left[\sigma_{zz} + \int_0^r t\sigma_{zz}(t)\,dt\,\frac{S^2(s)}{R^2(r)}\left(\frac{dn}{dr}\right)\right]\times$$

$$\times\frac{R(r)\,dr}{\sqrt{R^2(r) - S^2(s)}}. \qquad (23)$$

Optical retardation (23) consists of two terms: main retardation due to axial stress and additional one due curving of the ray. It has an additional

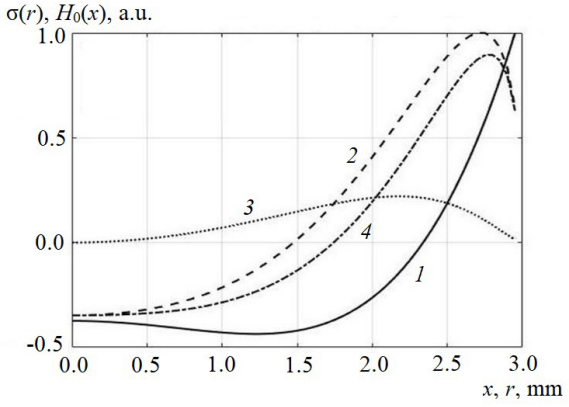

Fig. 5. The result of the residual stresses simulation (an example for using the polynomial datum on the sample of $R = 3$ mm); in addition to the axial stress curve (*1*), the curves of optical (*2*), additional (*3*) and main (*4*) retardations are presented

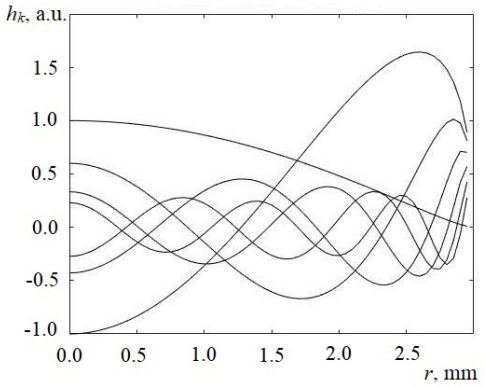

Fig. 6. Integrals $h_k(r)$ obtained on a basis of the first seven Zernike polynomials

term connected with ray deflection. The above algorithm is used for stress reconstruction

$$\sum_{n=1}^{N}\left[\hat{H}_0(s_n)-h_k(s_n)\sigma_{zz0}^{k}\right]^2=\min.$$

The graphs for the reconstruction of stresses in GRIN lenses made of zirconium-silicate ($n_0 = 1.54$) glasses are shown in Fig. 4 [23].

Fig. 5 shows the result of simulation of residual stresses by the polynomial datum for the case of $R = 3$ mm. Fig. 6 gives the retardations for the first seven Zernike polynomials.

Summary

In recent years, there has been a growing interest towards tomographic reconstruction of vector and tensor fields in the refracting medium [5, 6, 22]. We present the algorithm for reconstruction of residual stresses in GRIN lenses. From an experimental standpoint, implementation of the given method of reconstruction does not pose any particular difficulties and is conducted similarly to the case of the constant refractive index. The simplest examples of applications of this algorithm for the axial symmetric distribution of stresses are presented. The inversion algorithm provides a comparatively smooth stress distribution, produced by the ion-change technique. Including the radial dependences of the photoelasticity coefficients and elastic constants in GRIN structures in the algorithm for reconstructing stresses is the subject for further research.

Appendix

SCD of quasi-plane stresses

Let us consider a representation of quasi-plane stresses in terms of Zernike polynomials $R_k^m(r)$ [12], $m > 0$:

$$\sigma_{zz}(r,\varphi,z)=$$

$$=\sum_{m=1}\sum_{k=0}^{\infty}\left[\sigma_{zzm}^{kc}(z)\cos(m\varphi)+\right.$$
$$\left.+\sigma_{zzm}^{kc}(z)\sin(m\varphi)R_{m+2k}^{m}(r)\right],$$

$$\Phi(r,\varphi,z)=$$
$$=\sum_{m=1}\sum_{k=1}^{\infty}\left[f_m^{kc}(r,z)\cos(m\varphi)+\right.$$
$$\left.+f_m^{kc}(r,z)\sin(m\varphi)\right],$$

$$\tau(r,\varphi,z)=$$
$$=\sum_{m=1}\sum_{k=1}^{\infty}\left[\tau_m^{kc}(r,z)\cos(m\varphi)+\right.$$
$$\left.+\tau_m^{kc}(r,z)\sin(m\varphi)\right],$$

$$\sigma_{ij}(r,\varphi,z) = \sum_{m=1}\sum_{k=1}^{\infty}\left[\sigma_{ijm}^{kc}(r,z)\cos(m\varphi) + \sigma_{ijm}^{kc}(r,z)\sin(m\varphi)\right].$$

In the following, as evident from the context of the notation, the trigonometric functions are not written out:

$$f_m^{kc,s}(r,z) = \frac{-1}{2m}\left[C_k^m(r) + D_k^m(r)\right]\sigma_{zzm}^{kc,s}(z),$$

$$\tau_m^{kc,s}(\rho,z) = \frac{1}{2m}\left[C_k^m(r) + D_k^m(r)\right]\frac{\partial}{\partial z}\sigma_{zzm}^{kc,s}(z),$$

$$\sigma_{\rho\rho m}^{kc[s]}(r,z) = \frac{1}{2\rho^2}\left[(m+1)C_k^m(r) + (m-1)D_k^m(r)\right]\sigma_{zzm}^{kc[s]}(z) - \frac{1}{2m}\left[C_k^m(r) + D_k^m(r)\right]\frac{\partial^2}{\partial z^2}\sigma_{zzm}^{kc[s]}(z),$$

$$\sigma_{\rho\varphi m}^{kc[s]}(r,z) = \pm\frac{1}{2r^2}\left[(m+1)C_k^m(r) - (m-1)D_k^m(r)\right]\sigma_{zzm}^{kc[s]}(z)\begin{cases}\sin(m\varphi)\\ \left[\cos(m\varphi)\right]\end{cases},$$

$$\sigma_{\varphi\varphi m}^{kc[s]}(r,z) = R_{m+2k}^m(r)\sigma_{zzm}^{kc[s]}(z) - \sigma_{\rho\rho m}^{kc[s]}(r,z) - \frac{1}{m}\left[C_k^m(r) + D_k^m(r)\right]\frac{\partial^2}{\partial z^2}\sigma_{zzm}^{kc[s]}(z),$$

$$\sigma_{rzm}^{kc[s]}(r,z) = \frac{\partial}{\partial r}\tau_m^{kc,s}(r,z) = \frac{-1}{2\rho}\left[C_k^m(r) - D_k^m(r)\right]\frac{\partial}{\partial z}\sigma_{zzm}^{kc[s]}(z),$$

$$\sigma_{\varphi zm}^{ks[c]}(r,z) = \mp\frac{1}{2r}\left[C_k^m(r) + D_k^m(r)\right]\frac{\partial}{\partial z}\sigma_{zzm}^{kc[s]}(z)\begin{cases}\sin(m\varphi)\\ \left[\cos(m\varphi)\right]\end{cases},$$

where

$$C_k^m(r) = \frac{r}{2(2k+m+1)}\times\left[R_{m+2k+1}^{m+1}(r) - R_{m+2k-1}^{m+1}(r)\right],$$

$$D_k^m(\rho) = \frac{r}{2(2k+m+1)}\times\left[R_{m+2k-1}^{m-1}(r) - R_{m+2k+1}^{m-1}(r)\right].$$

In the case of an axial symmetric plane strain state ($m = 0$), the solution of the inverse thermoelastic problem can be represented in terms of Zernike polynomials $R_{2k}^0(r)$:

$$\sigma_{zz}(r) = \sum_{k=0}^{\infty}\sigma_{zz}^k R_{2k}^0(r),$$

$$\sigma_{\rho\rho}(r) = \sum_{k=1}^{\infty}\sigma_{zz}^k\sigma_{\rho\rho}^k(r),$$

$$\sigma_{\varphi\varphi}(r) = \sum_{k=1}^{\infty}\sigma_{zz}^k\sigma_{\varphi\varphi}^k(r),$$

$$\sigma_{\rho\rho}^k(r) = \frac{1}{\rho^2}\int_0^{\rho} tR_{2k}^0(t)\,dt = \frac{1}{2(2k+1)\rho}\left[R_{2k+1}^1(\rho) - R_{2k-1}^1(\rho)\right],$$

$$\sigma_{\varphi\varphi}^k(r) = R_{2k}^0 - \sigma_{\rho\rho}^k(r).$$

REFERENCES

1. **Yablon A.D.,** Recent progress in optical fiber refractive index profiling, Proceedings of the Optical Fiber Communication Conference/National Fiber Optic Engineers Conference, Los Angeles, USA. 6 – 10 March 2011, Paper OMF1. OSA Technical Digest (CD), Optical Society of America, 2011.

2. **Aben H., Ainola L., Anton J.,** Integrated photoelasticity for nondestructive residual stress measurements in glass, Optics and Lasers in Engineering. 33 (1) (2000) 49–64.

3. **Puro A., Aben H.,** Tensor field tomography for residual stress measurement in glass articles, Proceedings of the 7th European Conference on Non-Destructive Testing, Copenhagen, 26 – 29 May, 1998. NTD net. 3 (8) (1998) 2390–2397.

4. **Fuki A.A., Kravtsov Y.A., Naida O.N.,** Geometrical optics of weakly anisotropic media, Gordon and Breach Science Publishers, Amsterdam, 1998.

5. **Pfitzenreiter T., Schuster T.,** Tomographic reconstruction of the curl and divergence of 2D vector fields taking refractions into account, SIAM Journal on Imaging Sciences. 4 (1) (2011) 40–56.

6. **Svetov I.E., Derevtsov E.Yu., Volkov Yu.S., Schuster T.,** A numerical solver based on B-splines for 2D vector field tomography in a refracting medium, Mathematics and Computers in Simulation. 97 (March) (2014) 207–223.

7. **Puro A.E.,** Tomography in optically axisymmetric media, Optics and Spectroscopy. 124 (2) (2018) 278–284.

8. **Puro A., Karov D.,** Inverse problem of thermoelasticity of fiber gratings, Journal of Thermal Stresses. 39 (5) (2016) 500 – 512.

9. **Puro A., Karov D.,** Polarization tomography of residual stresses in cylindrical gradient-index lenses, Optics and Spectroscopy. 124 (5) (2018) 735–740.

10. **Born M., Wolf E.,** Principles of optics, 7th edition, Cambridge University Press, Cambridge, 2019.

11. **Puro A.,** Cormack-type inversion of exponential Radon transform, Inverse problems. 17 (1) (2001) 179–188.

12. **Puro A.,** Polarization tomography of the Tokamak plasma magnetic field, Optics and Spectroscopy. 116 (1) (2014) 122–129.

13. **Bieg B., Chrzanowski J., Kravtsov Y.A., Orsitto F.,** Main physical factors limiting the accuracy of polarimetric measurements in Tokamak plasma, Physics Procedia. 62 (2015) 107–112.

14. **Zeng G.L., Li Y.,** A discrete convolution kernel for No-DC MRI, Inverse Problems. 31 (8) (2015) 085006.

15. **Braun H., Hauck A.,** Tomographic reconstruction of vector fields, IEEE Transactions on Signal Processing. 39 (2) (1991) 464–471.

16. **Gardon R.,** Thermal tempering of glass, In the book "Glass Science and Technology, Vol. 5: Elasticity and Strength in Glasses", Edited by D.R. Uhlmann, N.J. Kreidl. Ch. 5, Academic Press, New York (1980) 145–213.

17. **Pretzier G., Jäger H., Neger T., et al.,** Comparison of different methods of Abel inversion using computer simulated and experimental side-on data, Zeitschrift für Naturforschung. A. 47a (1992) 955–970.

18. **Fricker P.,** Zernike polynomials and functions (orthogonal basis on the unit circle), Version 1.3.0.1. (6.84 KB), 2016, https://se.mathworks.com/ matlabcentral/ fileexchange /7687-Zernike-polynomials.

19. **Killer C.,** Abel inversion algorithm, Fourier-based reconstruction of an unknown radial distribution assuming cylindrical symmetry version 1.5.0.0 (4.17 KB), 2016. https://au.mathworks.com/matlabcentral/ fileexchange/43639-abel-inversion-algorithm.

20. **Wang Y.,** Radial gradient index rod containing Li^+, Acta Photonica Sinica. 31 (7) (2002) 897–900.

21. **Adam J.A., Pohrivchak M.,** Evaluation of ray-path integrals in geometrical optics, International Journal of Applied and Experimental Mathematics. 1 (2) (2016) 108.

22. **Ramadan W.A., Wahba H.H., Shams El-Din M.A.,** Two-dimensional refractive index and birefringence profiles of a graded index bent optical fibre, Optical Fiber Technology. 36 (July) (2017) 115–124.

23. **Karov D.D.,** Polyarizatsionnaya tomografiya napryazhyonnogo sostoyaniya v gradientno-op-

ticheskikh strukturakh [Polarizing tomography of a stressed state in the gradient-optical structures], PhD Thesis, Specialty 01.04.04, Peter the Great St. Petersburg Polytechnic University, St. Petersburg, 2012 (in Russian), http://fizmathim.com/read/369384/a?#?page=16.

Received 01.10.2020, accepted 14.10.2020.

THE AUTHORS

KAROV Dmitry D.
Peter the Great St. Petersburg Polytechnic University
29 Politechnicheskaya St., St. Petersburg, 195251, Russian Federation
dmkarov@yandex.ru

PURO Alfred E.
Euroacademy
4 Mustamäe tee, Tallinn, 10621, Estonia
alfredpuro@gmail.com

СПИСОК ЛИТЕРАТУРЫ

1. **Yablon A.D.** Recent progress in optical fiber refractive index profiling // Proceedings of the Optical Fiber Communication Conference/National Fiber Optic Engineers Conference. Los Angeles, USA. 6 – 10 March 2011. Paper OMF1. OSA Technical Digest (CD). Optical Society of America, 2011.

2. **Aben H., Ainola L., Anton J.** Integrated photoelasticity for nondestructive residual stress measurements in glass // Optics and Lasers in Engineering. 2000. Vol. 33. No. 1. Pp. 49–64.

3. **Puro A., Aben H.** Tensor field tomography for residual stress measurement in glass articles // Proceedings of the 7th European Conference on Non-Destructive Testing. Copenhagen. 26 – 29 May, 1998. NTD net. 1998. Vol. 3. No. 8. Pp. 2390–2397.

4. **Fuki A.A., Kravtsov Y.A., Naida O.N.** Geometrical optics of weakly anisotropic media. Amsterdam: Gordon and Breach Science Publishers, 1998. 182 p.

5. **Pfitzenreiter T., Schuster T.** Tomographic reconstruction of the curl and divergence of 2D vector fields taking refractions into account // SIAM Journal on Imaging Sciences. 2011. Vol. 4. No. 1. Pp. 40–56.

6. **Svetov I.E., Derevtsov E.Yu., Volkov Yu.S., Schuster T.** A numerical solver based on B-splines for 2D vector field tomography in a refracting medium // Mathematics and Computers in Simulation. 2014. Vol. 97. March. Pp. 207–223.

7. **Пуро А.Э.** Томография в оптически осесимметричных средах // Оптика и спектроскопия. 2018. Т. 124. № 2. С. 280–286.

8. **Puro A., Karov D.** Inverse problem of thermoelasticity of fiber gratings // Journal of Thermal Stresses. 2016. Vol. 39. No. 5. Pp. 500–512.

9. **Пуро А.Э., Каров Д.Д.** Поляризационная томография остаточных напряжений в цилиндрических граданах // Оптика и спектроскопия. 2018. Т. 124. № 5. С. 700–705.

10. **Борн М., Вольф Э.** Основы оптики. Пер. с англ. 2-е изд. М.: Наука. Гл. ред. физ.-мат. литры, 1973. 720 с.

11. **Puro A.** Cormack-type inversion of exponential Radon transform // Inverse problems. 2001. Vol. 17. No. 1. Pp. 179–188.

12. **Пуро А.Э.** Поляризационная томография магнитного поля плазмы Токамака // Оптика и спектроскопия. 2014. Т. 116. № 1. С. 135–142.

13. **Bieg B., Chrzanowski J., Kravtsov Y.A., Orsitto F.** Main physical factors limiting the ac-

curacy of polarimetric measurements in Tokamak plasma // Physics Procedia. 2015. Vol. 62. Pp. 107–112.

14. **Zeng G.L., Li Y.** A discrete convolution kernel for No-DC MRI // Inverse Problems. 2015. Vol. 31. No. 8. P. 085006.

15. **Braun H., Hauck A.** Tomographic reconstruction of vector fields // IEEE Transactions on Signal Processing. 1991. Vol. 39. No. 2. Pp. 464–471.

16. **Gardon R.** Thermal tempering of glass // Glass Science and Technology. Vol. 5. Elasticity and Strength in Glasses. Edited by D.R. Uhlmann, N.J. Kreidl. Chapter 5. New York: Academic Press, 1980. Pp. 145–213.

17. **Pretzier G., Jäger H., Neger T., Philipp H., Woisetschläger J.** Comparison of different methods of Abel inversion using computer simulated and experimental side-on data // Zeitschrift für Naturforschung. A. 1992. Vol. 47a. Pp. 955–970.

18. **Fricker P.** Zernike polynomials and functions (orthogonal basis on the unit circle). Version 1.3.0.1. (6.84 KB). 2016. https://se.mathworks.com/ matlabcentral/ fileexchange /7687-Zernike-polynomials.

19. **Killer C.** Abel inversion algorithm. Fourier-based reconstruction of an unknown radial distribution assuming cylindrical symmetry version 1.5.0.0 (4.17 KB). 2016. https://au.mathworks.com/matlabcentral/ fileexchange/43639-abel-inversion-algorithm.

20. **Wang Y.** Radial gradient index rod containing Li^+ // Acta Photonica Sinica. 2002. Vol. 31. No. 7. Pp. 897–900.

21. **Adam J.A., Pohrivchak M.** Evaluation of ray-path integrals in geometrical optics // International Journal of Applied and Experimental Mathematics. 2016. Vol. 1. No. 2. P. 108.

22. **Ramadan W.A., Wahba H.H., Shams El-Din M.A.** Two-dimensional refractive index and birefringence profiles of a graded index bent optical fibre // Optical Fiber Technology. 2017. Vol. 36. July. Pp. 115–124.

23. **Каров Д.Д.** Поляризационная томография напряженного состояния в градиентно-оптических структурах. Дисс. ... канд. физико-математических наук. Специальность 01.04.04. СПб.: Санкт-Петербургский политехнический университет Петра Великого, 2012. 182 с.

Статья поступила в редакцию 01.10.2020, принята к публикации 14.10.2020.

СВЕДЕНИЯ ОБ АВТОРАХ

КАРОВ Дмитрий Дмитриевич – *кандидат физико-математических наук, доцент Высшей школы прикладной физики и космических технологий Санкт-Петербургского политехнического университета Петра Великого, Санкт-Петербург, Российская Федерация.*

195251, Российская Федерация, г. Санкт-Петербург, Политехническая ул., 29

dmkarov@yandex.ru

ПУРО Альфред Эдуардович – *доктор физико-математических наук, профессор Евроакадемии, г. Таллинн, Эстония.*

10621, Эстония, г. Таллинн, ул. Мустамяэ, 4

alfredpuro@gmail.com

© Санкт-Петербургский политехнический университет Петра Великого, 2020